or acetaldehyde failed to alter significantly the rate of decomposition.

The product (**5**) displays a reversible couple at 1.02 V, a single broad NMR resonance at 3.95 ppm, and an IR stretch at 1899 cm^{-1}. $[Os(NH_3)_5(CO)]^{2+}$ has been previously characterized,[17] and the electrochemical, NMR, and infrared data are in excellent agreement with those obtained for **5**. Methane is thought to be the other major product.

$$[Os(NH_3)_5(\eta^2\text{-}CH_3CHO)]^{2+} = [Os(NH_3)_5(CO)]^{2+} + CH_4$$

In an attempt to verify this, the thermal decomposition of the aldehyde complex was investigated with a direct-insertion mass spectrometer to analyze the volatile pyrolysis products. In this experiment a sample of $[Os(NH_3)_5(\eta^2\text{-}CH_3CHO)](TFMS)_2$ was heated under vacuum at a rate of 20 °C/min to a final temperature of 350 °C.

Between 180 and 200 °C there was a sudden rise in ionization current, and the corresponding mass spectrum contained peaks at m/e 16 (100%), 17 (97%), 18 (39%), and 15 (37%). These are consistent with the fragmentation pattern for methane.[30]

Reactivity with Formaldehyde. Recently, a great deal of attention has been given to π-bound formaldehyde complexes because of their suspected role as intermediates in a homogeneous Fisher–Tropsch cycle.[2b,c] More generally, the fixation of formaldehyde to a metal center is considered to be a primary goal in generating metal-promoted transformations of a C_1 molecule.[2e] When a DME solution of $[Os(NH_3)_5(TMB)]^{2+}$ (TMB = 1,2,3,4-tetramethylbenzene), a synthetic precursor to $[Os(NH_3)_5(L)]^{2+}$,[31] is treated with a dilute gas stream of CH_2O, an immediate color change to deep red occurs, but NMR and cyclic voltammetry give no indication of either an η^2-bound formaldehyde complex or $[Os(NH_3)_5(CO)]^{2+}$. This reaction is currently under investigation.

(29) Generated in situ by the addition of $[FeCp_2]PF_6$.
(30) See reference 18, p 1.
(31) Harman, W. D.; Taube, H. *Inorg. Chem.* **1987**, *26*, 2917.

Conclusion

Although η^2-bound aldehyde and ketone complexes are uncommon, we have found that these complexes are quite stable with pentaammineosmium(II), a strongly π-basic metal center. Placing bulky substituents on the ketone destabilizes the η^2-isomer, whereas conjugated ketones are found to stabilize this bonding mode. Although the oxidation potentials for these species are quite positive, an $\eta^2 \rightarrow \eta^1$ isomerization renders them potent reducing agents. The utilization of the facile one-electron oxidation of these complexes has led to a determination of their specific rates and free energies of isomerization.

Pentaammineosmium(II) was also found to interact with the aromatic portion of the phenones investigated. In these complexes, the metal coordinates η^2 to the arene interrupting its aromaticity. In the case of benzophenone, this complex eventually isomerizes to the thermodynamically favored η^2-ketone isomer.

A combination of the high affinity for π-acid ligands, kinetic stability associated with latter transition-metal complexes, and an easily accessible oxidation state make pentaammineosmium(II) ideally suited for the study of π-complexation and back-bonding.

Acknowledgment. Support of this work by National Science Foundation Grants CHE85-11658 and CHE84-14329 (400-MHz NMR) and National Institutes of Health Grant GM13638-20 is gratefully acknowledged.

Registry No. **1**, 105164-48-5; **2a**, 113161-71-0; **2b**, 113161-73-2; **3**, 113161-67-4; **4**, 113161-69-6; $[Os(NH_3)_5(TFMS)](TFMS)_2$, 83781-30-0; $[Os(NH_3)_5(FBN)](TFMS)_2$, 113161-76-5; $[Os(NH_3)_5(\eta^2\text{-}CH_3COCH_3)]^{2+}$, 105164-47-4; $[Os(NH_3)_5(\eta^2\text{-cyclopentanone})]^{2+}$, 113161-77-6; $[Os(NH_3)_5(\eta^2\text{-cyclobutanone})]^{2+}$, 113161-78-7; $[Os(NH_3)_5(\eta^2\text{-}CH_3CH_2COCH_3)]^{2+}$, 113161-79-8; $[Os(NH_3)_5(\eta^2\text{-}(CH_3)_2CHCOCH_3)]^{2+}$, 113161-80-1; $[Os(NH_3)_5(\eta^1\text{-}(CH_3)_3CCOCH_3)]^{2+}$, 113161-81-2; $[Os(NH_3)_5(\eta^2\text{-PhCOC}(CH_3)_3)]^{2+}$, 113161-66-3; $[Os(NH_3)_5(\eta^2\text{-PhCOPh})]^{2+}$, 113161-72-1; $[Os(NH_3)_5(DMA)]^{3+}$, 113161-82-3; $[Os(NH_3)_5(CH_3CN)]^{3+}$, 83781-32-2; $[Os(NH_3)_5(CH_2CH_2)]^{3+}$, 113161-83-4; DMPP, 938-16-9; $[Os(NH_3)_5(PhCN)](TFMS)_2$, 113161-74-3; benzophenone, 119-61-9; acetaldehyde, 75-07-0; formaldehyde, 50-00-0.

Rubidium X-ray Absorption (EXAFS and XANES) Studies of Rb^- and Complexed Rb^+ in Alkalides and Electrides

Odette Fussa-Rydel,[†] James L. Dye,*[†] and Boon K. Teo[‡,§]

Contribution from the Department of Chemistry, Michigan State University, East Lansing, Michigan 48824, and AT&T Bell Laboratories, Murray Hill, New Jersey 07971.
Received July 24, 1986

Abstract: The Rb K-edge X-ray absorption near-edge structure (XANES) and extended X-ray absorption fine structure (EXAFS) spectra of compounds with stoichiometries RbNa(18C6), Rb(18C6), Rb_2(18C6), RbNa(15C5)$_2$, Rb(15C5)$_2$, Rb(15C5), RbK(C222), CsRb(18C6)$_2$, RbK(18C6), RbK(15C5)$_2$, CsRb(15C5)$_2$, Rb(C222), and Rb_2(C222) have been measured and interpreted. The XANES spectra provide a means of identifying the oxidation state of the rubidium-containing species in these salts. The compounds Cs^+(18C6)$_2$,Rb^-, K^+(C222),Rb^-, and Cs^+(15C5)$_2$,Rb^- are pure rubidides. They show no detectable EXAFS, consistent with the large size of Rb^-. The spectra of Rb^+(18C6),Na^-, Rb^+(15C5)$_2$,Na^-, Rb^+(15C5)$_2$,e^-, and Rb^+(C222),e^- are similar to (but not identical with) those of the model compounds Rb^+(18C6),Br^-·2H_2O and Rb^+(18C6)SCN^-. The compounds Rb^+(15C5)$_2$,Rb^-, Rb^+(18C6),Rb^-, Rb(18C6), Rb^+(C222),Rb^-, RbK(18C6), and RbK(15C5)$_2$,e^- are mixtures that contain both the complexed rubidium cation and the rubidide anion. The EXAFS data for Rb^+(15C5)$_2$,e^- and Rb^+(15C5)$_2$,Rb^- indicate local structures around the rubidium cation similar to that of Rb^+(15C5)$_2$,Na^-, a sodide whose crystal structure has been determined by X-ray diffraction. The radial distribution functions of the compounds Rb^+(18C6),X^- indicate different conformations of the 18-crown-6 ring in different salts.

A number of compounds that contain novel types of anionic species have been synthesized in our laboratory.[1-4] Alkalides contain alkali metal anions, while electrides contain stoichiometrically trapped electrons as the anions. In both types of salts

[†] Michigan State University.
[‡] AT&T Bell Laboratories.
[§] Current address: Department of Chemistry, University of Illinois, Chicago, Chicago, IL 60680.

(1) Dye, J. L.; Ceraso, J. M.; Lok, M. T.; Barnett, B. L.; Tehan, F. J. *J. Am. Chem. Soc.* **1974**, *96*, 608-609.
(2) Dye, J. L. *Angew. Chem., Int. Ed. Engl.* **1979**, *18*, 587-598.

0002-7863/88/1510-2445$01.50/0

the cation consists of an alkali metal cation complexed by an organic polyether cage compound such as a cryptand or a crown ether. Representative complexants are the bicyclic polyoxa diamine cryptand[2.2.2], designated C222 (**1**), and the macrocyclic polyethers 18-crown-6 (**2**; 18C6) and 15-crown-5 (**3**; 15C5).

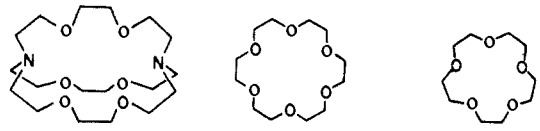

1 2 3

Several spectroscopic methods have been used to identify and characterize the species present in alkalides and electrides. Although it is a relatively straightforward task to determine the stoichiometry of the salts, identifying the species present is not so easy. Optical spectra of thin films have been helpful,[5-7] but the absorption peak of a given alkali metal anion can shift as much as 1500 cm^{-1} from one salt to another.[8] Furthermore, the optical peak of the trapped electron varies from one salt to another and can be easily confused with an absorption peak from Cs^- or Rb^-. Alkali metal magic angle sample spinning NMR has been extremely useful in identifying species[8-10] since the large diamagnetic shift of M^- is characteristic of the anions. For example, the Rb^- anion has been identified in polycrystalline samples of Rb^+(15-crown-5)$_2Rb^-$, Cs^+(15-crown-5)$_2$,Rb^-, and Cs^+(8-crown-6)$_2$,Rb^- as well as samples containing K, Rb, and 15-crown-5.[10] Because of extreme quadrupolar line broadening, however, Rb^+C cannot be observed by MAS-NMR methods.

To be able to fully characterize the alkalides and electrides, it is necessary to know their structures. The "parent" compound Na^+(C222),Na^- was characterized by single-crystal X-ray diffraction methods.[11] Its structure is similar to that of the corresponding iodide.[12] Recently the structures of two other sodides, $Cs^+(18C6)_2$,Na^- and $Rb^+(15C5)_2$,Na^-, have been determined[13] as well as the structure of the electride $Cs^+(18C6)_2$,e^-.[14] Structural studies of most other alkalides and electrides have, until very recently, been hindered by thermal instabilities and extreme air sensitivities, as well as by the difficulty in preparing suitable single crystals.

Our interest in the characterization and structural elucidation of alkalides and electrides led us to use the combined techniques of extended X-ray absorption fine structure (EXAFS) and X-ray absorption near-edge structure (XANES). The strength of these combined techniques has been demonstrated recently by a number of studies that permitted structural determinations not possible by conventional diffraction techniques.[15] We report here an extension of a preliminary study[16] of a series of rubidium-containing alkalides and electrides by Rb K-edge EXAFS and XANES spectroscopy. Compounds with the stoichiometry RbNa(18C6), Rb(18C6), Rb_2(18C6), RbNa(15C5)$_2$, Rb(15C5)$_2$, Rb(15C5), RbK(C222), CsRb(18C6)$_2$, RbK(18C6), RbK-(15C5)$_2$, CsRb(15C5)$_2$, Rb(C222), and Rb_2(C222) were studied. When only a single crystalline phase is present, the combined use of EXAFS and XANES spectroscopies has provided a method of identifying the rubidium-containing species. For example, powdered samples of overall stoichiometry Rb(C222) and Rb_2-(C222) were presumed to be the electride and rubidide, respectively. The absence of the Rb^- NMR peak expected for a rubidide[10] made the assignment uncertain, however. As described in this paper, rubidium XANES studies provided confirmation of the existence of both the electride and the rubidide. The most important result of the EXAFS study was the observation that the rubidium cation in the crown ether or cryptate complex has nearly the same environment in alkalides and electrides as it has with ordinary anions such as SCN^- and Br^-.

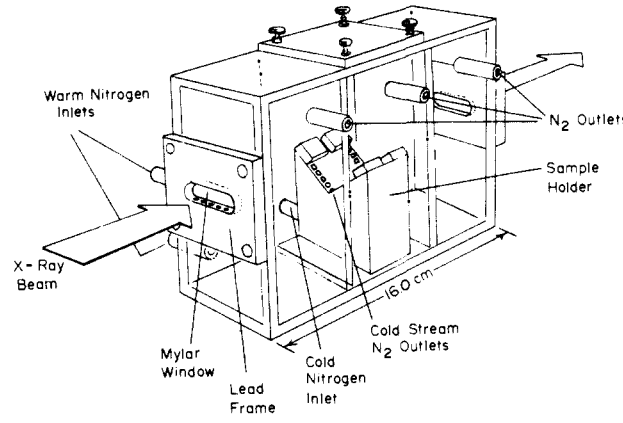

Figure 1. Sample holder cryostat used in the X-ray absorption measurements.

Experimental Section

X-ray Absorption Measurements. Transmission X-ray measurements for Rb (K-edge at 15.201 KeV) were made at the Cornell High Energy Synchrotron Source (CHESS)[17] on the C2 EXAFS beam line. The synchrotron used electron–positron energies of 5.3 GeV and a storage ring injection current of 30 mA. A channel-cut Si (220) single-crystal monochromator, detuned by 50% for harmonic rejection, was used. The spectra were recorded from 15.000 to 16.230 keV. For the XANES region (15.175–15.225 keV), the measurements were made at 0.5-eV intervals, while for the EXAFS region 1.2-eV intervals were used. The beam size was 1 × 13 mm^2. The incident and transmitted beam intensities were measured by ionization chambers of 8- and 30-cm lengths, respectively, filled with argon (flow type). The monochromator was calibrated with an yttrium foil (K-edge at 17.037 keV[18]).

Sample Preparation and Handling. Polycrystalline (powder) samples of alkalides and electrides were synthesized in our laboratory as described previously[1-4] and stored at reduced temperatures in sealed glass ampules. These ampules were opened just prior to each scan. To prevent decomposition, all sample handling was done in inert atmosphere (N_2 gas) glovebags equipped with a cold well immersed in a tray of liquid nitrogen. The polycrystalline samples were mixed with dry boron nitride powder by using a cold agate mortar and pestle and pressed to form a uniform pellet of suitable thickness ($\mu\chi \sim 1.0$).

In order to maintain the samples cold and under an inert atmosphere during data collection, a sample holder cryostat was designed. This air-tight cryostat, shown in Figure 1, was made of acrylic sheets and contains three compartments through which prepurified nitrogen gas flows. The central compartment contains the sample holder and is maintained at temperatures between −35 and −45 °C during data collection. None of the compounds studied exhibit structural changes within this temperature range. The two adjacent compartments are continuously flushed with dry nitrogen gas at room temperature to ensure a frost-free beam path. Mylar tape was used on all windows in the X-ray path. A frame of lead adhesive tape around the beam entry and exit ports

(3) Van Eck, B.; Le, L. D.; Issa, D.; Dye, J. L. *Inorg. Chem.* **1982**, *21*, 1966–1980.
(4) Dye, J. L. In *Progress in Inorganic Chemistry*; Lippard, S. J. Ed.; Wiley-Interscience: New York, 1984; Vol. 32, pp 327–447.
(5) Dye, J. L.; Yemen, M. R.; DaGue, M. G.; Lehn, J.-M. *J. Chem. Phys.* **1978**, *68*, 1665–1670.
(6) Dye, J. L.; DaGue, M. G.; Yemen, M. R.; Landers, J. S.; Lewis, H. L. *J. Phys. Chem.* **1980**, *84*, 1096–1103.
(7) Landers, J. S.; Dye, J. L.; Stacy, A.; Sienko, M. J. *J. Phys. Chem.* **1981**, *85*, 1096–1099.
(8) Ellaboudy, A.; Tinkham, M. L.; Van Eck, B.; Dye, J. L. *J. Phys. Chem.* **1984**, *88*, 3852–3855.
(9) Ellaboudy, A.; Dye, J. L.; Smith, P. B. *J. Am. Chem. Soc.* **1983**, *105*, 6490–6491.
(10) Tinkham, M. L.; Ellaboudy, A.; Dye, J. L.; Smith, P. B. *J. Phys. Chem.* **1986**, *90*, 14–16.
(11) Tehan, F. J.; Barnett, B. L.; Dye, J. L. *J. Am. Chem. Soc.* **1974**, *96*, 7203–7208.
(12) Moras, D.; Weiss, R. *Acta Crystallogr., Sect. B: Struct. Crystallogr. Cryst. Chem.* **1973**, *B29*, 396–399.
(13) Dawes, S. B.; Fussa, O.; Ward, D.; Dye, J. L., to be submitted for publication.
(14) Dawes, S. B.; Ward, D. L.; Huang, R. H.; Dye, J. L. *J. Am. Chem. Soc.* **1986**, *108*, 3534–3535.
(15) See, for example: (a) Rao, K. J.; Wong, J.; Weber, M. J. *J. Chem. Phys.* **1983**, *78*, 6228–6237. (b) Pan, H. K.; Knapp, G. S.; Cooper, S. L. *Colloid Polym. Sci.* **1984**, *262*, 734–746.
(16) Fussa, O.; Kauzlarich, S.; Dye, J. L.; Teo, B. K. *J. Am. Chem. Soc.* **1985**, *107*, 3727–3728.
(17) For a description of CHESS, see: Batterman, B. W. In *EXAFS Spectroscopy: Techniques and Applications*; Teo, B. K., Joy, D. C., Eds.; Plenum: New York, 1981.
(18) Bearden, J. A. *Rev. Mod. Phys.* **1967**, *39*, 78–124.

Table I. Normalized Areas of White Line (cm × 10^2)

compound	pristine sample	dec sample	compound	pristine sample	dec sample
RbCl	19		Rb(18C6)	16	30
RbBr	15		$RbK(15C5)_2$	16	34
$Rb^+(18C6),SCN^-$	27		RbK(18C6)	10	35
$Rb^+(18C6),Br^-\cdot 2H_2O$	25		$Rb^+(C222),Rb^-$	14	33
$Rb^+(15C5)_2,Na^-$	29	34	$Rb^+(C222),e^-$	22	29
$Rb^+(15C5)_2,e^-$	32	39	$K^+(C222),Rb^-$	4	27
$Rb^+(18C6),Na^-$	19	29	$Cs^+(18C6)_2,Rb^-$	1	29
$Rb^+(15C5)_2,Rb^-$	18	31	$Cs^+(15C5)_2,Rb^-$	7	38
$Rb^+(18C6),Rb^-$	12	30			

ensured proper alignment of the cryostat with respect to the beam. A polyethylene glovebag around the whole assembly (but not in the beam path) prevented contamination of the atmosphere in the cryostat when changing samples.

Before the first sample was inserted, the sample chamber was purged with dry nitrogen at room temperature. After this, a cold nitrogen stream was used in the central chamber. The sample holder has a series of channels that allowed the stream of cold gas to flow directly over the sample, thus ensuring that it was maintained cold and frost-free during the scan.

The salts $Rb^+(18C6),SCN^-$ and $Rb^+(18C6),Br^-\cdot 2H_2O$ are stable and were used as reference compounds to model the structure of the complexed rubidium cation. The structures of these two salts are known from single-crystal X-ray diffraction studies.[19,20]

After each run, the alkalide and electride samples were allowed to react with air to produce the corresponding hydroxides. Spectra of the oxidized materials were then scanned for comparison with the pristine samples.

Data Analysis. Standard methods of data analysis were used.[21] The experimental energy threshold values were chosen as the photon energies at half-height of the edge jump. These threshold energies were found to be 15195 ± 1 eV for all those compounds that contain either the simple rubidium cation or the complexed rubidium cation in the form Rb^+-(18C6) or $Rb^+(15C5)_2$. However, because the calibration foil (yttrium) has an edge energy nearly 2 keV higher than that of rubidium, the absolute accuracy of the threshold energy could not be ascertained. The background was removed by using five sets (ca. 2.92 $Å^{-1}$ each) of cubic spline functions. The EXAFS data were Fourier transformed, filtered, and curve fit with the phenomenological EXAFS equation[21] by using a least-squares minimization technique. The best fit based on theory (BFBT) and fine adjustment based on models (FABM)[21a] formalisms were used.

Results and Discussion

The rubidium K-edge X-ray absorption spectrum, $\mu\chi$ vs E (eV), of $Rb^+(15C5)_2,Na^-$ is shown in Figure 2a. This spectrum exhibits features typical of those alkalides and electrides that contain the complexed rubidium cation. Similar features, namely, a sharp K-edge absorption threshold resonance (white line) and fine structure extending up to 300 eV above the edge, are observed in the spectra of the model compounds $Rb^+(18C6),SCN^-$, and $Rb^+(18C6),Br^-\cdot 2H_2O$, which also contain the rubidium cation complexed by a crown ether ring. Very different features are observed in the EXAFS spectrum of $Cs^+(18C6)_2,Rb^-$, shown in Figure 2b. The intensity of the white line is considerably smaller, and the fine structure is absent. These differences in the spectra point to the difference in the oxidation state and environment of rubidium in these two compounds. The spectrum of the rubidide, $Cs^+(18C6)_2,Rb^-$, is remarkably similar to that of Kr gas.[22] The white line, which is due to transitions from core to vacant bound excited states and is a measure of the density of such states, is virtually absent, indicating the low density of such states in Rb^-. In addition, there is no discernible EXAFS, a result of the large

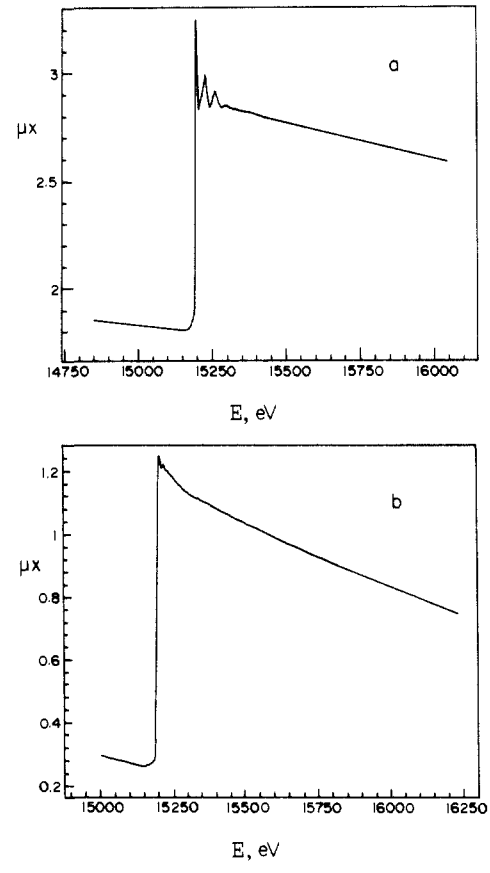

Figure 2. Rubidium K-edge transmission X-ray absorption spectrum, $\mu\chi$ vs E (eV), of (a) $Rb^+(15C5)_2,Na^-$ and (b) $Cs^+(18C6)_2,Rb^-$.

size of Rb^-. The radius of this anion has been estimated[2] to be 3.4 Å, which would give a minimum interionic distance of 4.9 Å. The similarity in the spectra of Kr gas and $Cs^+(18C6)_2,Rb^-$ confirms the assumption that the rubidide anion in the solid is a large spherical anion with no atomic or ionic species in close proximity. This type of environment for alkali metal anions has been observed in the crystal structures of the three sodides referred to earlier. Additional evidence in support of this description of the rubidide anion has been obtained from results of magic angle sample spinning NMR experiments.[10]

XANES and White-Line Areas. The rubidide anion has an electronic configuration that consists of a krypton core and two electrons in the 5s orbital. For K-edge absorption, where the initial state has s symmetry and zero angular momentum, the dipole selection rule of $\Delta l = \pm 1$ allows only a single important final state of $l = 1$ with p symmetry.[22] The observed white line in complexed Rb^+ can therefore be attributed largely to a dipole-allowed transition from the 1s to a bound 5p orbital in the molecular cage defined by the first shell of ligands. It is the confining effect of the cage potential in "inner-well" unoccupied orbitals that enhances the oscillator strength of transitions to these orbitals.[23] In the

(19) Dobler, M.; Phizackerley, R. P. *Acta Crysallogr. Sect. B: Struct. Crystallogr. Cryst. Chem.* **1974**, *B38*, 2746–2748.
(20) Fussa, O.; Ward, D. L.; Dye, J. L., to be submitted for publication.
(21) (a) Teo, B. K.; Antonio, M. R.; Averill, B. A. *J. Am. Chem. Soc.* **1983**, *105*, 3751–3762. (b) Teo, B. K. *Acc. Chem. Res.* **1980**, *13*, 412–419. (c) Teo, B. K., Joy, D. C., Eds. *EXAFS Spectroscopy: Techniques and Applications*; Plenum: New York, 1981; pp 13–58. (d) Teo, B. K.; Shulman, R. G.; Brown, G. S.; Meisner, A. E. *J. Am. Chem. Soc.* **1979**, *101*, 5624–5631.
(22) Stern, E. A.; Heald, S. M. In *Handbook on Synchrotron Radiation*; Koch, E. E., Ed.; North-Holland: Amsterdam, The Netherlands, 1983; Vol. 1, pp 955–1014.
(23) Kutzler, F. W.; Natoli, C. R.; Misener, D. K.; Doniach, S.; Hodgson, K. O. *J. Chem. Phys.* **1980**, *73*, 3274–3288.

rubidide, Rb^-, where the cage is no longer present, the 5p orbital is very diffuse, thereby giving rise to a weak oscillator strength for the dipole transition. In this regard, it should be pointed out that electrons in the 5p orbital in complexed Rb^+ are also much more tightly bound than in Rb^-.

These observations led to the conclusion that the areas of the white lines can be used to diagnose the oxidation state(s) of the absorbing rubidium species in alkalides and electrides. With this in mind, the areas of the white lines for all compounds studied were measured and normalized to unit edge jump. The results are presented in Table I. The units (10^{-2} cm) are arbitrary and will be disregarded in the discussion that follows.

The compounds that contain only the complexed rubidium cation exhibit the largest white-line areas, with values ranging from 19 to 27, close to those of the oxidized samples (27–38). On the other hand, the smallest white-line areas are those of compounds that only contain rubidium as an anion, such as $Cs^+(18C6)_2,Rb^-$, $K^+(C222),Rb^-$, and $Cs^+(15C5)_2,Rb^-$. Between these two extremes are compounds that contain both the complexed rubidium cation and the rubidide anion, such as $Rb^+(18C6),Rb^-$, $Rb^+(C222),Rb^-$, and $Rb^+(15C5)_2,Rb^-$. The white-line areas, A = 12, 14, and 18, respectively, are approximately half the values observed for similar salts that contain only complexed Rb^+. This is consistent with the fact that in these rubidides only half the rubidium exists as Rb^+. Finally, the heteronuclear alkalides, $RbK(15C5)_2$ and RbK(18C6) (A = 16 and 10), exhibit values lower than expected for the complexed rubidium cation but higher than those of pure rubidides. This suggests that they are mixtures of all or some of the salts Rb^+C,K^-, K^+C,Rb^-, Rb^+C,Rb^-, and K^+C,K^-, where C represents the complexant. Magic angle sample spinning NMR data on K^- and Rb^- agree with this conclusion.[10,24]

In general, the $Rb^+(15C5)_2,X^-$ salts, which have Rb^+ sandwiched in a three-dimensional trap formed by two 15-crown-5 rings, exhibit larger white-line areas than those of either $Rb^+(18C6),X^-$ salts or simple rubidium salts such as Rb^+,Cl^-. In the former nonsandwich crown ether salts, the rubidium cation is displaced from the mean plane of the ligand and is thus exposed to the anions. These results suggest that when the anion can come into contact with Rb^+, it can donate electronic charge more readily and thus decrease the density of available final states for the 1s → 5p transition.

The XANES results show that it is generally possible to distinguish electrides from rubidides. They show unequivocally that both $Rb^+(15C5)_2,e^-$ and $Rb^+(18C5)_2Rb^-$ can be synthesized as can $Rb^+(C222),e^-$ and $Rb^+(C222),Rb^-$. The identification of the rubidium-containing species present in the salt of nominal stoichiometry Rb(18C6) poses a special problem, however. This stoichiometry represents more than one possible complex, i.e., $Rb^+(18C6),e^-$, a pure electride, or $Rb^+(18C6)_2,Rb^-$, a rubidide with two crown ether rings complexing the cation. It is also possible that $Rb^+(18C6),Rb^-$ and 18C6 coprecipitate. Initial efforts to identify the species present involved optical spectroscopy studies of thin films of the compound prepared from a solution of the crystals in methylamine.[25] However, a definitive identification of the species present was not obtained. The films exhibited broad absorption bands at 11 600 and 8900 cm^{-1}, characteristic of Rb^- and the trapped electron, respectively, but the same features were also observed in the optical spectra of films made from $Rb_2(18C6)$. Rubidium-87 solid-state magic angle sample spinning NMR experiments[10,25] have identified the presence of the rubidide anion in some alkalides. Some samples prepared from rubidium and 18C6 showed an NMR signal of Rb^- while others did not. Thus, neither optical nor NMR spectra could be used to identify the species present in powders of stoichiometry Rb(18C6).

Both XANES and EXAFS data for Rb(18C6) suggest the presence of the rubidium anion in the crystals. There is only a small increase in the relative area of the white line measured for Rb(18C6) compared to that of $Rb^+(18C6),Rb^-$. The value falls in the intermediate range of areas and corresponds to mixtures of Rb^+ and Rb^-. Thus, it is likely that the crystallites under study contain mixtures of both rubidium electride and rubidium rubidide as suggested by the NMR and optical data. However, an alternate possibility cannot be ruled out, namely, that the small white-line area in Rb(18C6) is the result of large electron-density donation from the trapped electron to the exposed cation.

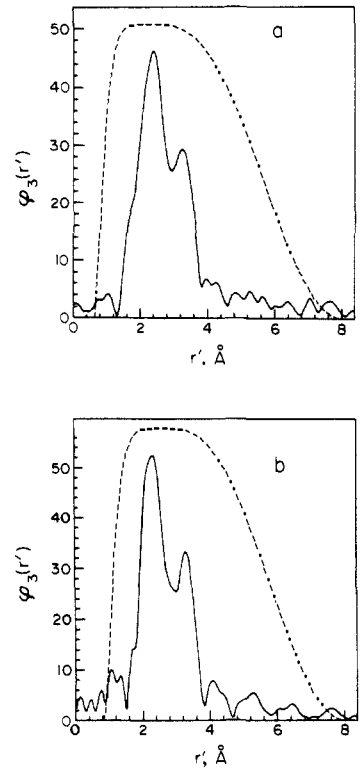

Figure 3. Fourier transforms (solid curves), $\phi_3(r')$ vs r' (Å) (before phase shift correction), of the background-subtracted $k^3\chi(k)$ vs k rubidium K-edge transmission EXAFS data and filtering windows (dashed curves) for (a) $Rb^+(15C5)_2,Na^-$ and (b) $Rb^+(15C5)_2,e^-$.

Edge Shifts. The absorption edge threshold values for complexed rubidium in compounds that contain the $Rb^+(18C6)$ or $Rb^+(15C5)_2$ moieties were compared to those of salts that contain rubidium only in the anionic state. For example, in the pure rubidide, $Cs^+(18C6)_2,Rb^-$, the edge is shifted to lower energies by 3 eV, compared to that of compounds that contain only Rb^+, reflecting the smaller energy required to remove the 1s electron to an outer state in the anionic species. The magnitude of the shift is, however, smaller than would have been predicted for a change in charge of two units (from Rb^+ to Rb^-) in a completely ionic environment[26] or in the gas phase. A possible explanation is that the magnitude of electron-pair donation from the oxygens of the crown ether to the complexed rubidium cation is such that the actual negative charge in the vicinity of the cation is not as different from that of Rb^- as would be deduced from the formal charge difference.

EXAFS and Structures. The Fourier transforms of the normalized EXAFS $k^3\chi(k)$ vs k for the rubidium K-edge in $Rb^+(15C5)_2,Na^-$ and $Rb^+(15C5)_2,e^-$ are shown in Figure 3. These have not been corrected for the phase shift, so the peaks appear at distances that are somewhat shorter than the true distances. Note that these Fourier transforms show two broad peaks centered at 2.5 and 3.5 Å. The structure of $Rb^+(15C5)_2,Na^-$ has been determined by using single-crystal X-ray diffraction methods.[13] In this compound the rubidium cation is sandwiched between two 15-crown-5 rings and has as nearest neighbors 10 oxygen atoms from the crown rings (Rb–O, 2.99–3.07 Å; average, 3.01 Å). The cation is fully protected by the rings and has no contact with the anion. The closest approach between the cation and the sodide

(24) Tinkham, M. L.; Dye, J. L. *J. Am. Chem. Soc.* **1985**, *107*, 6129–6130.
(25) Ellaboudy, A. Ph.D. Dissertation, Michigan State University, 1984.
(26) Shulman, R. G.; Yafet, Y.; Eisenberger, P.; Blumberg, W. E. *Proc. Natl. Acad. Sci. U.S.A.* **1976**, *73*, 1384–1388.

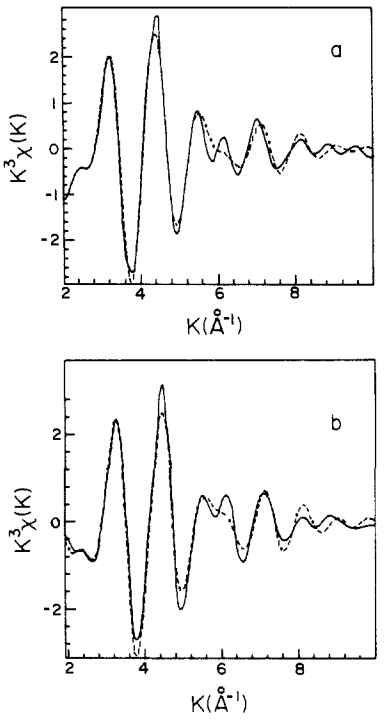

Figure 4. BFBT nonliner least-squares curve fit (dashed curve) of the Fourier-filtered $k^3\chi(k)$ vs k EXAFS spectrum (solid curve) for (a) $Rb^+(15C5)_2,Na^-$ and (b) $Rb^+(15C5)_2,e^-$.

anion is 7.49 Å.[13] Even longer distances are expected for Rb^+ to anion contacts in $Rb^+(15C5)_2,Rb^-$. EXAFS cannot provide such long distances, however. The peak observed at 3.5 Å corresponds to a shell of carbon nieghbors from the 15-crown-5 ring. There are 20 such neighbors at an average distance of 3.82 Å. The similarities in the positions and magnitudes of the peaks suggest a similar local structure for the rubidium cation in $Rb^+(15C5)_2,Na^-$ and $Rb^+(15C5)_2,e^-$. As expected for an electride salt, the FT's of $Rb^+(15C5)_2,e^-$ do not show distances corresponding to the anion.

The dashed curves shown in Figure 3 are the window functions used to filter the backscattering contributions from the distance space (Å) before Fourier inverse transformation of the data back to k-space (Å^{-1}). The Fourier-filtered data, $k^3\chi$ vs k in the region from 2.0 to 10.0 Å are shown as solid curves in Figure 4. The filtered EXAFS spectra were then resolved into two terms to account for a shell of oxygen nearest neighbors and an outer shell of carbon neighbors and were least-squares fit with the single-electron, single-scattering formalism of the EXAFS effect (eq 1),[21]

$$k^3\chi(k) = \sum_j B_j F_j(k_j) k_j^2 \exp(-2\sigma_j^2 k_j^2) \frac{\sin[2k_j r_j + \phi_j(k_j)]}{r_j^2} \quad (1)$$

where σ_j, r_j, and k_j denote the Debye–Waller factor, the interatomic distance, and the photoelectron wave vector, respectively. Theoretical amplitude $F_j(k_j)$ and phase $\phi_j(k_j)$ functions were used for j corresponding to oxygen and carbon.[27,28] The scale factor B_j is related to the number of atoms N_j by $B_j = S_j N_j$, where S_j is the amplitude reduction factor.

S_j has a k dependence given by eq 2 where $S_o^2(k)$ takes into account inelastic losses at the absorbing atom and $\lambda(k)$ is the inelastic electron mean free path in a scattering process by neighboring atoms j.[21] If the amplitude reduction factor S_j was

$$S_j(k) = S_o^2(k)\, e^{-2r_j/\lambda(k)} \quad (2)$$

known, the coordination number, N_j, could be calculated from the fitted scale factor B_j. There is, however, no reliable a priori calculation of $S_j(k)$ available for these systems. This makes it impossible to calculate coordination numbers by the BFBT procedure. Correlations among the Debye–Waller factors and the scale factors for model compounds do permit the estimation of coordination numbers[21] as given in Table III.

Table II. Best Fit (Based on Theoretical Functions) Least-Squares-Refined Interatomic Distances r (Å), Debye–Waller Factors σ(Å), and Energy Threshold Differences ΔE_o^P (eV)

compound	term	r	σ	ΔE_o^P
$Rb^+(15C5)_2,Na^-$	Rb–O	2.99	0.155	2.43
	Rb–C	3.87	0.120	4.34
$Rb^+(15C5)_2,e^-$	Rb–O	2.97	0.150	3.14
	Rb–C	3.88	0.105	4.50
$Rb^+(15C5)_2,Rb^-$	Rb–O	2.96	0.146	3.30
	Rb–C	3.88	0.104	5.08
$Rb^+(18C6),SCN^-$	Rb–O	2.99	0.126	3.52
	Rb–S	3.48	0.0916	2.35
	Rb–C	3.96	0.0728	7.55
$Rb^+(18C6),Br^-\cdot 2H_2O$	Rb–O	3.00	0.132	3.79
	Rb–Br	3.46	0.0769	0.0160
	Rb–C	3.94	0.0769	6.43
$Rb^+(18C6),Na^-$	Rb–O	2.93	0.135	3.88
	Rb–C	3.85	0.0952	6.18
Rb(18C6)	Rb–O_1	2.99	0.144	4.15
	Rb–O_2	3.64	0.0664	−0.120
	Rb–C	3.95	0.0664	8.25
$Rb^+(18C6),Rb^-$	Rb–O_1	2.90	0.123	3.81
	Rb–O_2	3.60	0.0474	−0.342
	Rb–C	3.91	0.0474	8.69

Table III. Fine Adjustment (Based on Model Compounds) to Best Fit Based on Theory Results for Interatomic Distances r (Å) and Coordination Numbers (N)

compound	term	r^a	N
$Rb^+(15C5)_2,Na^-$	Rb–O	3.009[b]	10.00[b]
	Rb–C	3.818[b]	20.00[b]
$Rb^+(15C5)_2,e^-$	Rb–O	2.97	10.46
	Rb–C	3.82	19.38
$Rb^+(15C5)_2,Rb^-$	Rb–O	2.95	12.50
	Rb–C	3.80	24.74
$Rb^+(18C6),SCN^-$	Rb–O	3.024[c]	6.00[c]
	Rb–C	3.803[c]	12.00[c]
$Rb^+(18C6),Br^-\cdot 2H_2O$	Rb–O	3.01	4.75
	Rb–C	3.81	10.97
$Rb^+(18C6),Na^-$	Rb–O	2.95	5.66
	Rb–C	3.73	12.74
Rb(18C6)	Rb–O	2.99	7.36
	Rb–C	3.77	17.37
$Rb^+(18C6),Rb^-$	Rb–O	2.92	7.36
	Rb–C	3.75	16.80

[a] Standard deviations 0.05–0.11 Å. [b] Average interatomic distances from single-crystal X-ray diffraction results.[13] [c] Average interatomic distances from single-crystal X-ray diffraction results.[19]

The best fits based upon theory, BFBT (dashed curves), are depicted in Figure 4. The resulting best fit (BFBT) least-squares refined parameters are presented in Table II. The structural similarity of the $Rb^+(15C5)_2$ moiety in the sodide, electride, and rubidide, suggested by the Fourier-transformed EXAFS spectra, is confirmed by the similarities in the Rb^+–O and Rb^+–C distances and the corresponding Debye–Waller factors. The relatively large values of σ for Rb^+–O and Rb^+–C result not only from thermal vibrations but also from the spread in Rb^+–O and Rb^+–C distances. A more detailed discussion of the Debye–Waller factors is given below.

The data were further refined by using the fine adjustment based on models (FABM) formalism.[21a] The correlation plots used to obtain these values are available.[29] The resulting distances, presented in Table III, agree with those from the BFBT method.

The radial distribution functions (not corrected for phase shift) for $Rb^+(18C6),SCN^-$, $Rb^+(18C6),Na^-$, $Rb^+(18C6),Rb^-$, and Rb(18C6) are presented in Figure 5. For the thiocyanate salt, peaks are observed at 2.5, 3.1, and 3.6 Å, which correspond to

(27) Teo, B. K.; Lee, P. A. *J. Am. Chem. Soc.* **1979**, *101*, 2815–2832.
(28) Teo, B. K. *J. Am. Chem. Soc.* **1981**, *103*, 3990–4001.
(29) Fussa, O. Ph.D. Dissertation, Michigan State University, 1986.

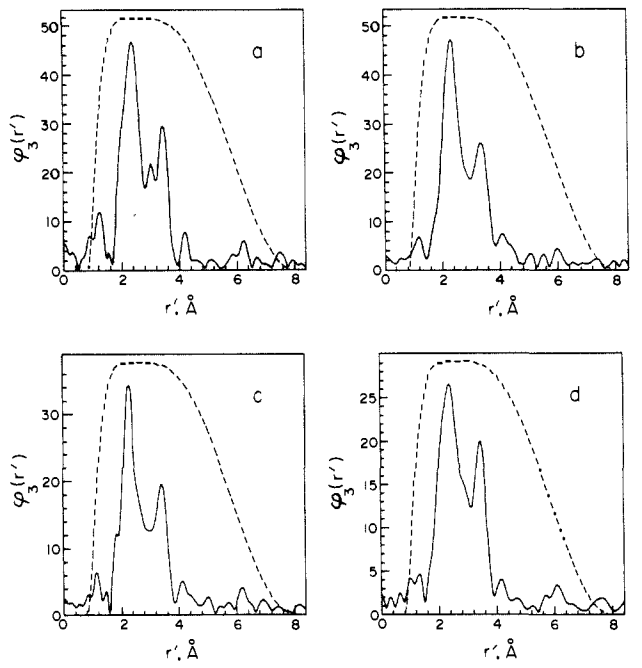

Figure 5. Fourier transforms (solid curves), $\phi_3(r')$ vs r' (Å) (before phase shift correction), of the background-subtracted $k^3\chi(k)$ vs k rubidium K-edge transmission EXAFS data for (a) $Rb^+(18C6),SCN^-$, (b) $Rb^+(18C6),Na^-$, (c) $Rb^+(18C6),Rb^-$, and (d) Rb(18C6).

Rb–O, Rb–S, and Rb–C distances, respectively. In this compound, Rb^+ is coordinated to six oxygens of the crown ether (Rb–O, 2.93–3.15 Å) and to two thiocyanate anions [Rb–N(S), 3.23 and 3.31 Å].[19] In the case of the sodide, $Rb^+(18C6),Na^-$, there is no peak in the radial distribution function at distances between those of Rb–O and Rb–C. This is because, by contrast with the model thiocyanate, there are no close contacts between Rb^+ and the sodium anion, and only the contacts to oxygens and carbons of the complexing agent can be detected by EXAFS. On the basis of their sizes, even direct contact between Rb^+ and Na^- would correspond to a distance of 4.0 Å. In this case, the spectrum was Fourier-filtered, resolved into two components, $k^3\chi_O$ and $k^3\chi_C$, and fit with eq 1 for j = O, C, as was done previously for the $Rb^+(15C5)_2,X^-$ series. The FT's of $Rb^+(18C6),Br^-\cdot 2H_2O$, $Rb^+(18C6),Rb^-$, and Rb(18C6) show the characteristic peaks at 2.5 and 3.5 Å, which represent the Rb–O and Rb–C distances, respectively. In the case of the bromide, a peak at 2.7 Å corresponds to coordination to the oxygens of the water molecules of the dihydrate. The FT's of $Rb^+(18C6),Rb^-$ and Rb(18C6) have a small shoulder at 3.0 Å. This shoulder cannot be attributed to scattering by the Rb^- anion, since the observed distances are too short. Instead, it is believed to arise from a lengthening of one or more of the Rb–O distances because of distortion in the 18-crown-6 ring. It is known that the 18-crown-6 molecule is flexible and can adopt different conformations compatible with the coordination requirements of the specific complex. The fact that the FT's of $Rb^+(18C6),Rb^-$ and Rb(18C6) are similar, but not identical, suggests, in agreement with the XANES results, that the latter is a mixture of an electride and a rubidide.

After Fourier-filtering, a "difference" Fourier technique was used to resolve the data for compounds with three sets of interatomic distances. This difference technique permits the separation of minor components from the major components in EXAFS.[30] To obtain a difference EXAFS spectrum, the filtered data are first fit in k-space with a model containing the dominant term(s) in the spectrum. The resulting fit is subtracted from the data, yielding a spectrum that contains the minor components and some residual background. This difference spectrum is then Fourier-transformed, and the minor components are Fourier filtered and back-transformed to yield a filtered difference spectrum in k-space. The difference spectrum is then fitted with a model that corresponds to the minor components in the original EXAFS spectrum. In the analysis of the EXAFS data for $Rb^+(18C6),SCN^-$, $Rb^+(18C6),Br^-\cdot 2H_2O$, $Rb^+(18C6),Rb^-$, and Rb(18C6), the fitted spectra were resolved into two components, $k^3\chi_O$ and $k^3\chi_{A/C}$, which could then be curve fit with a three term (j, O, A, C) backscattering formulation. Here, A represents the shell of neighbors located between the oxygen and carbon shells; that is, A = SCN^- and Br^- for $Rb^+(18C6),SCN^-$ and $Rb^+(18C6),Br^-\cdot 2H_2O$, respectively, and A = oxygen for $Rb^+(18C6),Rb^-$ and Rb(18C6). The resulting values for the best fit parameters are listed in Table II, and all of the graphics are presented elsewhere.[29] The FABM results are given in Table III. For Rb(18C6) and $Rb^+(18C6),Rb^-$ the values obtained from the fit with two Rb–O terms suggest that the first Rb–O shell of neighbors occurs at approximately the same distance as in the models while the second shell appears at ~3.60 Å. It was not possible to further refine these values with the FABM method because there are no known reference compounds that exhibit this type of coordination.

It should also be noted that in both $Rb^+(18C6),Rb^-$ and Rb(18C6) a reduction in the magnitude of the FT is present. This is expected for $Rb^+(18C6),Rb^-$ since only half of the rubidium is present as the cation and Rb^- has no significant contribution to the EXAFS spectrum. The reduction in the EXAFS amplitude of Rb(18C6) suggests that this too may be a rubidide, perhaps the sandwich compound $Rb^+(18C6)_2,Rb^-$. However, no other sandwich complexes of Rb^+ with 18C6 are known, and a more likely explanation is that the sample was a mixture of compounds.

The FT of $Cs^+(18C6)_2,Rb^-$ yields no discernible peaks above the background. This confirms the view obtained from the XANES studies that Rb^- is a large, spherical anion with no neighboring species within bonding distance. For the systems that contained mixtures of complexed rubidium cations and rubidide anions a proportionate reduction in the amplitude of the $k^3\chi(k)$ vs k data is evident. This feature can be used in addition to the XANES spectrum to indicate the presence of rubidium anions in a sample.

EXAFS Amplitudes. In all the radial distribution functions shown, the overall magnitudes of the peaks for these complexes are smaller than usually obtained from EXAFS spectroscopy. This is consistent with the nature of the complexation of alkali metals by cryptands and crown ethers. The magnitude of the radial structure function is accounted for in part by the factor $\exp[-2\sigma_j^2k^2]$ in the amplitude component of the EXAFS equation (eq 1). This Debye–Waller factor has two components, σ_{stat} and σ_{vib}, due to static disorder and thermal vibrations respectively.[21c] It can be described by eq 3.

$$\sigma = [\sigma_{stat}^2 + \sigma_{vib}^2]^{1/2} \quad (3)$$

For the type of coordination in these alkali metal complexes, both contributions are rather large. The cation is complexed loosely by the ligating oxygens, the bonds are relatively weak, and there is appreciable vibrational motion even at the low temperatures employed for data collection. Some room-temperature EXAFS scans of the model compounds were very noisy, and their quality proved unacceptable for data analysis. The static contribution to the Debye–Waller factor is also relatively large. The crystallographic data show that the distances between the rubidium cation and the oxygen atoms are not all equal.[13,19] In addition, in some cases more than one stable conformation for the crown ether is allowed, and this causes disorder in the complexation. This type of disorder has been observed in the structures of $Rb^+(15C5)_2,Na^-$[13] and $Cs^+(15C5)_2,I^-$.[31] The static contribution to the Debye–Waller factor can be estimated by eq 4 for N neighbors

$$\sigma_{stat} \approx [\sum_{j=1}^{N} [(r_j - r_0)^2/N]] \quad (4)$$

of the same type, for which $r_j - r_0$ is the deviation from the mean

(30) Teo, B. K. *EXAFS: Basic Principles and Data Analysis*; Springer: Berlin, 1986; p 139.

(31) Dawes, S.; Ward, D. L.; Dye, J. L., to be submitted for publication.

distance r_0. When this expression is used with the crystallographic data for the six Rb–O distances[19] in $Rb^+(18C6)\cdot SCN(8C6),SCN^-$, the Rb–O contribution to σ_{stat} was found to be 0.083 Å.

The value of σ_{vib} cannot be independently calculated because the necessary vibrational data are not available. When the experimental Debye–Waller factor is used, it can be estimated to be 0.043 Å. Similar calculations for $Rb^+(18C6),Br^-\cdot 2H_2O$[20] give 0.091 and 0.041 Å for σ_{stat} and σ_{vib}, respectively.

The reduced EXAFS amplitudes obtained for these complexes are also due to the relatively large distances between the rubidium cation and the nearest shell of oxygen neighbors from the ligand (3.00 Å). This causes a reduction in the amplitude because of the r^{-2} dependence of the EXAFS function (eq 1).

Conclusions

The combined use of XANES and EXAFS has permitted the identification and structural characterization of rubidium-containing alkalides and electrides. The white-line areas provide a means of identifying these new products as pure rubidides, electrides, or mixtures. These XANES studies have been especially valuable in identifying the rubidium-containing species in heteronuclear alkalides such as $Rb^+(18C6),Na^-$, $Cs^+(18C6)_2,Rb^-$, and $K^+(C222),Rb^-$. In other cases, they have shown the presence of mixtures of alkalides such as in $RbK(15C5)_2$ and RbK(18C6). They have also been valuable in the study of those compounds that contain only rubidium and the complexant. For example, they have allowed the characterization of $Rb^+(15C5)_2,e^-$ as a pure electride and of $Rb^+(15C5)_2,Rb^-$ as a rubidide with complexed rubidium as the cation. These assignments would not have been possible with optical spectroscopy or ^{87}Rb magic angle sample spinning NMR studies. For the compound Rb(18C6), however, a final determination was not possible, and the results suggest that this stoichiometry might correspond to a mixture of species.

The alkalide and electride salts that contain $Rb^+(18C6)$ are especially difficult to crystallize, and for these, the results of this study provide the only available structural information at present. These data suggest that the conformations of 18-crown-6 in $Rb^+(18C6),Rb^-$ and in Rb(18C6) are slightly different from those in the models $Rb^+(18C6),SCN^-$ and $Rb^+(18C6),Br^-\cdot 2H_2O$, while that of $Rb^+(18C6),Na^-$ is essentially the same as those in the models. The structures of the $Rb^+(15C5)_2,X^-$ complexes are similar to that of the model compound, $Rb^+(15C5)_2,Na^-$, which has a rubidium cation sandwiched between two 15-crown-5 rings. The rubidide anion, Rb^-, has been shown to be a large anion with no nearest neighbors at detectable distances.

Acknowledgment. This work was supported by National Science Foundation Solid-State Chemistry Grants DMR 79-21979 and DMR 84-14154. CHESS is supported by NSF Grant DMR 81-12811. We gratefully acknowledge S. M. Kauzlarich for helpful discussions and S. B. Dawes, M. K. Faber, R. H. Huang, and J. Kim for their valuable assistance in collecting the data. We also thank the technical staff at CHESS for their help.

Registry No. Rb, 7440-17-7; Rb^-, 26396-76-9; RbCl, 7791-11-9; RbBr, 7789-39-1; $Rb^+(18C6),SCN^-$, 38295-06-6; $Rb^+(18C6),Br^-$, 96503-66-1; $Rb^+(15C5)_2,Na^-$, 89462-37-3; $Rb^+(15C5)_2,e^-$, 113380-65-7; $Rb^+(18C6),Na^-$, 89462-38-4; $Rb^+(15C5)_2,Rb^-$, 96503-70-7; $Rb^+(18C6),Rb^-$, 96503-68-3; Rb(18C6), 96503-72-9; $Rb^+(C2222),Rb^-$, 57450-09-6; $Rb^+(C222),e^-$, 96503-75-2; $K^+(C222),Rb^-$, 113380-66-8; $Cs^+(18C6)_2,Rb^-$, 96503-67-2; $Cs^+(15C5)_2,Rb^-$, 99582-52-2.

Singlet Molecular Oxygen: Not a Major Product of the Reaction between Tris(2,2′-bipyridine)ruthenium(3+) and Superoxide Radical Anions†

Q. G. Mulazzani,*‡ M. Ciano,‡ M. D'Angelantonio,‡ M. Venturi,‡,§ and M. A. J. Rodgers*⊥

Contribution from the Istituto di Fotochimica e Radiazioni d'Alta Energia, Consiglio Nazionale delle Ricerche, Via de' Castagnoli 1, 40126 Bologna, Italy, Dipartimento di Chimica "G. Ciamician", Via Selmi 2, 40126 Bologna, Italy, and Center for Fast Kinetics Research, University of Texas, Austin, Texas 78712. *Received September 9, 1987*

Abstract: Time-resolved infrared luminescence and computer-aided kinetic modeling have been used to demonstrate that singlet molecular oxygen, O_2 ($^1\Delta_g$), is not formed during the electron-transfer reaction between $Ru(bpy)_3^{3+}$ and $O_2^{\bullet-}$ ions in aqueous media. This is in direct contrast to what has been claimed earlier. As far as we are able to determine, the only singlet oxygen formed photolytically in a reaction mixture containing $Ru(bpy)_3^{2+}$, MV^{2+}, and O_2 is that generated by energy transfer between $^*Ru(bpy)_3^{2+}$ and ground-state oxygen. Radiolytic and electrochemical measurements have established that the bleaching of the singlet oxygen trap $ADPA^{2-}$, which occurs with a quantum yield of 0.12 ± 0.01 when H_2O or D_2O solutions containing $Ru(bpy)_3^{2+}$, MV^{2+}, O_2, and $ADPA^{2-}$ are photolyzed, is to be attributed to the oxidation of $ADPA^{2-}$ by $Ru(bpy)_3^{3+}$; from the computer modeling of the system a rate constant value of $\simeq 10^7$ $M^{-1}s^{-1}$ for the latter reaction has been evaluated.

It has been recently claimed[1] that the electron-transfer reaction between $Ru(bpy)_3^{3+}$ (bpy = 2,2′-bipyridine) and $O_2^{\bullet-}$ quantitatively generates singlet oxygen O_2 ($^1\Delta_g$) instead of the ground state O_2 ($^3\Sigma_g^-$). The two reactants were generated by the laser flash or steady-state photolysis of a system containing $Ru(bpy)_3^{2+}$, methylviologen (1,1′-dimethyl-4,4′-bipyridinium ion, MV^{2+}), and oxygen. The excitation of $Ru(bpy)_3^{2+}$ generates $^*Ru(bpy)_3^{2+}$ (reaction 1), which decays (reaction 2) with lifetimes of 0.62 and 1.02 μs in H_2O and D_2O, respectively.[2] In the absence of O_2, $^*Ru(bpy)_3^{2+}$ is quenched by MV^{2+} (reaction 3); the products of that reaction undergo electron back-transfer (reaction 4). In the

† Presented in part at the 4th International Congress on Oxygen Radicals, University of California at San Diego, LaJolla, CA, June 27–July 3, 1987.
‡ Istituto di Fotochimica e Radiazioni d'Alta Energia.
§ Dipartimento di Chimica "G. Ciamician".
⊥ Center for Fast Kinetics Research.

(1) Miller, S. S.; Zahir, K.; Haim, A. *Inorg. Chem.* **1985**, *24*, 3978–3980 and references therein.
(2) Kalyanasundaram, K. *Coord. Chem. Rev.* **1982**, *46*, 159–244.

0002-7863/88/1510-2451$01.50/0